Single-molecule imaging reveals distinct effects of ligands on CCR5 dynamics depending on its dimerization status

Fanny Momboisse[1], Giacomo Nardi[2], Philippe Colin[3], Melany Hery[1], Nelia Cordeiro[1], Olivier Schwartz[1], Nathalie Sauvonnet[5], Fernando Arenzana-Seisdedos[4], Thibault Lagache[2*], Bernard Lagane[3], Jean-Christophe Olivo-Marin[2], Anne Brelot[1*]

[1] : Institut Pasteur, Université de Paris, CNRS UMR3569, Virus and Immunity Unit, F-75015 Paris, France.

[2] : Institut Pasteur, Université de Paris, CNRS UMR 3691, BioImage Analysis Unit, F-75015 Paris, France.

[3] : Infinity, Université de Toulouse, CNRS, INSERM, UPS, 31024 Toulouse Cedex 03, France.

[4] : Institut Pasteur, Université de Paris, INSERM U1108, Viral Pathogenesis Unit, F-75015 Paris, France.

[5] : Institut Pasteur, Université de Paris, Group Intracellular Trafficking and Tissue Homeostasis, F-75015 Paris, France.

*To whom correspondence may be addressed:
Email: anne.brelot@pasteur.fr; thibault.lagache@pasteur.fr

Competing Interests: The authors declare that no competing interests exist.

Abstract

G protein-coupled receptors (GPCR) are present at the cell surface in different conformational and oligomeric states. However, how these states impact GPCRs biological function and therapeutic targeting remains incompletely known. Here, we investigated this issue in living cells for the CC chemokine receptor 5 (CCR5), a major receptor in inflammation and the principal entry co-receptor for Human Immunodeficiency Viruses (HIV-1). We used TIRF microscopy and an original statistical method to track and classify the motion of different receptors subpopulations. We showed a diversity of ligand-free forms of CCR5 at the cell surface constituted of various oligomeric states and exhibiting transient Brownian and restricted motions. These forms were stabilized differently by distinct ligands. In particular, agonist stimulation restricted the mobility of CCR5 and led to its clustering, a feature depending on β-arrestin, while inverse agonist stimulation exhibited the opposite effect. These results suggest a link between receptor activation and immobilization. Applied to HIV-1 envelope glycoproteins gp120, our quantitative analysis revealed agonist-like properties of gp120s. Distinct gp120s influenced CCR5 dynamics differently, suggesting that they stabilize different CCR5 conformations. Then, using a dimerization-compromized mutant, we showed that dimerization (i) impacts CCR5 precoupling to G proteins, (ii) is a pre-requisite for the immobilization and clustering of receptors upon activation, and (iii) regulates receptor endocytosis, thereby impacting the fate of activated receptors. This study demonstrates that tracking the dynamic behavior of a GPCR is an efficient way to link GPCR conformations to their functions, therefore improving the development of drugs targeting specific receptor conformations.

Introduction

G protein-coupled receptors (GPCRs), also known as 7TM (seven transmembrane helical) receptors, represent the largest group of cell surface receptors in humans that transduce chemical signals from the extracellular matrix into the cell. They constitute one of the primary drug target classes (Pierce et al., 2002).

GPCRs exist in different subpopulations at the cell surface, in part due to differential post-translational modifications (Patwardhan et al., 2021; Scurci et al., 2021) and arrangements of receptor loops and transmembrane domains (Deupi & Kobilka, 2010). Receptor activation and G protein coupling indeed involves a series of conformational changes from an inactive to an active state (Ahn et al., 2021). Coupling to different G proteins or to other protein transducers (*e.g.* arrestins), as well as receptor oligomerization expand the diversity of conformational states (Seyedabadi et al., 2019; Sleno & Hebert, 2018). Molecular dynamics along with biophysical and structural studies brought to light this variety of GPCR arrangements and showed how binding of different ligands can stabilize or select different receptor conformations, which can in turn activate different signaling pathways (Ahn et al., 2021). This concept of “functional selectivity” (or “biased agonism”) opens the possibility to develop therapies specifically targeting a selected receptor conformation, thereby increasing the effectiveness of drugs and reducing their adverse effects (Seyedabadi et al., 2019).

The nature and proportion of the different forms of GPCRs vary depending on their environment. This is likely to regulate the functional properties of the receptors (Colin et al., 2018; Patwardhan et al., 2021). Few studies, however, confirmed this diversity of receptors in living cells and investigated its regulation in time and space (Calebiro et al., 2013; Gormal et al., 2020; Kasai et al., 2018; Martinez-Munoz et al., 2018; Sungkaworn et al., 2017; Veya et al., 2015). In this study, we tracked the chemokine receptor CCR5

at the single molecule level to access its dynamic behavior at the plasma membrane and identify the stoichiometry and the functional properties of the various receptor forms.

CCR5 is a class A GPCR expressed on the surface of hematopoietic and non-hematopoietic cells. It is a key player in the trafficking of lymphocytes and monocytes/macrophages and has been implicated in the pathophysiology of multiple diseases, including viral infections and complex disorders with an inflammatory component (Brelot & Chakrabarti, 2018; Flanagan, 2014; Vangelista & Vento, 2017). In addition, the CCL5/CCR5 axis represents a major marker of tumor development (Aldinucci et al., 2020). CCR5 binds several chemokines, including CCL3, CCL4, and CCL5. Binding of chemokines results in conformational change of the receptor, which then activates intracellular signaling pathways and leads to cell migration (Flanagan, 2014). CCR5 also binds the envelope glycoprotein of HIV-1, then acting as the major HIV-1 entry co-receptor (Alkhatib et al., 1996; Brelot & Chakrabarti, 2018). One CCR5 allosteric ligand, maraviroc (MVC), is part of the anti-HIV-1 therapeutic arsenal (Dorr et al., 2005), although emergence of MVC-resistant variants has been identified in some patients (Tilton et al., 2010).

We and others showed the existence of various CCR5 populations present at the cell surface (Abrol et al., 2014; Berro et al., 2011; Colin et al., 2013; Colin et al., 2018; Fox et al., 2015; Jacquemard et al., 2021; Jin et al., 2014; Jin et al., 2018; Scurci et al., 2021). Computational analysis predicts that CCR5 can adopt an ensemble of low-energy conformations, each of which being differentially favored by distinct ligands and receptor mutations (Abrol et al., 2014). CCR5 conformations display distinct antigenic properties, which vary depending on cell types (Colin et al., 2018; Fox et al., 2015). The multiple conformations interact differently with distinct ligands (agonist, antagonist, HIV-1 envelope glycoprotein) and differ in their biological properties, HIV co-receptor functions,

and abilities to serve as therapeutic targets (Abrol et al., 2014; Colin et al., 2013; Colin et al., 2018; Jacquemard et al., 2021; Jin et al., 2014; Jin et al., 2018; Scurci et al., 2021). In particular, coupling to G proteins distinguishes CCR5 populations that are differently engaged by chemokines and HIV-1 envelope. This explains why HIV-1 escapes inhibition by chemokines (Colin et al., 2013). In this context, the improved capacity of chemokine analogs to inhibit HIV infection, as compared to native chemokines, is related to their ability to target a large amount of CCR5 conformations (Jin et al., 2014).

Like other receptors of this class, CCR5 forms homo- and hetero-dimers with other receptors, which contribute to the diversity of conformational states (Jin et al., 2018; Sohy et al., 2009). We identified three homo-dimeric organizations of CCR5 involving residues of transmembrane domain 5 (TM5) (Jin et al., 2018). Two dimeric states corresponded to unliganded receptors, whereas binding of the inverse agonist MVC stabilized a third state (Jin et al., 2018). CCR5 dimerization occurs in the endoplasmic reticulum, thereby regulating the receptor targeting to the cell surface (Jin et al., 2018). CCR5 dimerization also modulates ligand binding and HIV-1 entry into cells (Colin et al., 2018). MVC stabilizes CCR5 homodimerization, illustrating that CCR5 dimerization can be modulated by ligands (Jin et al., 2018), a feature shared with other chemokine receptors (Isbilir et al., 2020). Allosteric interaction within CCR2/CCR5 heterodimers is reported as well as cross-inhibition by specific antagonists (Sohy et al., 2009). This suggests that dimerization impacts therapeutic targeting.

To characterize the diversity of CCR5 subpopulations at the cell surface and to investigate the impact of CCR5 dynamics on its function, we tracked CCR5 fluorescent particles by total internal reflection fluorescence (TIRF) microscopy (Calebiro et al., 2013) and quantitatively classify their motion over time using an original statistical method. We described CCR5 mobility patterns both at the basal state and after ligand

123 binding (using two agonists, the inverse agonist MVC, and HIV-1 envelope
124 glycoproteins) and under conditions that modulate CCR5 / G protein coupling, β-arrestin
125 binding, and dimerization. This study provides novel insights into the organization of a
126 GPCR at the cell surface and the mechanisms regulating its signaling and fate after
127 activation.

128 ## Results

129 ### Statistical classification of receptor trajectories at the cell membrane

130 We generated a HEK 293 cell line stably expressing a low density of eGFP-CCR5 at the
131 cell surface (< 0.5 particles/μm^2), which is critical for single particle tracking on the
132 surface of living cells (Calebiro et al., 2013). We choose HEK 293 cells because they do
133 not express CCR5. Fusion of eGFP to the N-terminus of CCR5 does not alter cell
134 surface expression of the receptor or its intracellular trafficking (Boncompain et al.,
135 2019).

136 To study the dynamics of CCR5 as a single particle at the plasma membrane of living
137 cells, we used TIRF microscopy, which restricts the observation to the first 200 nm from
138 the coverslip. The acquisitions were carried out at 37 °C with a frequency of 30 Hz (1
139 image / 33 ms). From the movies obtained, we tracked the motion of the particles over
140 time using the *Spot tracking* plugin of the ICY software (Chenouard et al., 2013; de
141 Chaumont et al., 2012) (***Figure 1A-C***, ***Videos 1, 2, 3***, see Material and Methods).

142 The method generally used to evaluate the dynamics of a particle is based on Mean
143 Square Displacement (MSD) analysis (Qian et al., 1991). However, MSD is a global
144 analysis of particle trajectory that does not handle possible changes in particle motion. In
145 particular, it indicates whether the observed motion is standard Brownian motion and
146 computes the related diffusion coefficient of the trajectory, but it cannot characterize

more complex stochastic motions as the frequency of motion changes. In addition, the MSD analysis does not provide a statistical significance of classified motion. To robustly characterize the complex stochastic motions of single receptors at the cell membrane, we used an alternative statistical method. We first partitioned single receptor trajectories into small tracklets (with *N = 5* consecutive detections each) to mitigate the risk of tracking errors over long trajectories, and to detect potential motion changes between tracklets within each single receptor trajectory (***Figure 1D***). We first evaluated immobile objects and then used a robust statistical method to classify tracklet motion (see Material and Methods and ***Figure 1E-F***). Briefly, for each tracklet X, we computed the statistics $S(X,N)$ introduced in (Briane et al., 2018) that evaluate the ratio between the maximal distance reached by the tracklet particle from the initial point and the motion standard deviation. We then used the statistics $S(X,N)$ to classify each tracklet into one of the three following motion categories: *confined*, *Brownian*, or *directed* stochastic motion. For this, we computed *S(X,N)* for each tracklet and compared it to the quantiles $(q_\alpha, q_{1-\alpha})$, which are statistical reference values of Brownian motion at level α and $(1-\alpha)$. Quantiles of *S(X,N)* only depend on *N* and α (Briane et al., 2018), and can be evaluated independently of the characteristics of experimental trajectories. Finally, tracklets X were classified according to the associated stochastic motion: confined (if $S(X,N) < q(\alpha)$), Brownian (if $q(\alpha) \leq S(X,N) < q(1-\alpha)$), and directed motion (if $q(1-\alpha) \leq S(X,N)$) (***Figure 1-figure supplement 1***). We used this statistical classification procedure, with $\alpha = 0.05$, to characterize the dynamics of CCR5 particles at the cell membrane.

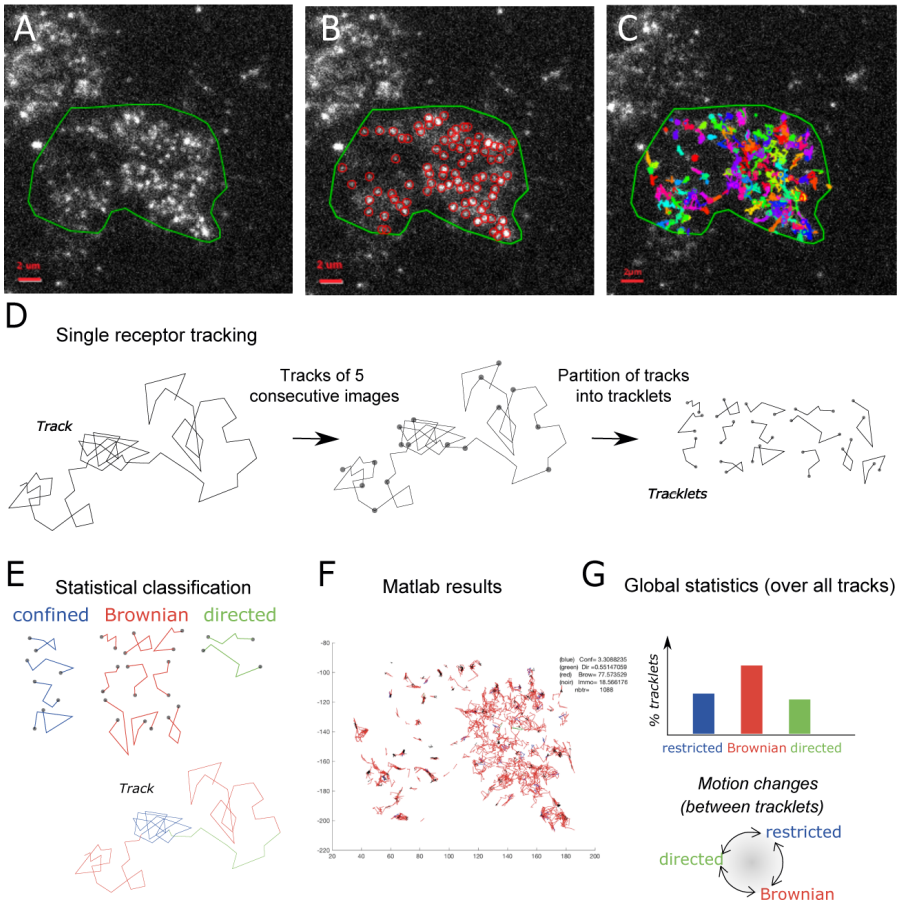

Figure 1. Single particle detection of eGFP-CCR5 using TIRF microscopy and analysis with the statistical method. (A) Distribution of eGFP-CCR5 stably expressed in HEK 293 cells. Imaging was acquired at 30 Hz. The region of interest defined by the green line is used for A-C and F. Analysis of movies was performed using the ICY software and (B) the *Spot detection* and (C) the *Spot tracking* pluggins. Scale bare 2 μm. (D) Single receptor tracks were partitionned into tracklets of 5 images each. (E) Analysis of tracks with the statistical method: tracklets were classified into confined, Brownian, and directed motion. (F) Results obtained from Matlab. (G) Pooled tracklets classification provided a global estimate of receptor dynamics and the number of motion changes along the track (transition rates). (Restricted motions: immobile and confined motions).

Video 1. TIRF movie of a cell stably expressing eGFP-CCR5-WT acquired at 30 Hz. The region of interest was defined by the green line**.**

Video 2. TIRF movie of the same cell as in video 1 analyzed using the Icy software. Red circles correspond to the detection of bright spots using the *Spot detection* pluggin.

Video 3. TIRF movie of the same cell as in video 1 and 2 analyzed using the Icy software and the *Spot tracking* pluggin. Colored lines correspond to the tracked spots.

Figure supplement 1. Validation of the statistical method using simulated trajectories.

CCR5 particles have different motions at the plasma membrane

We investigated CCR5 mobility in the basal state using the statistical method described above (***Figure 1***). The result of the classification of all the pooled tracklets provided a global estimate of the receptor dynamics, while the number of motion changes along the same trajectory gave us an estimate of the overall stability of the motion (***Figure 1G***).

In the basal state, the eGFP-CCR5 particles distributed homogeneously over the entire membrane surface (***Figure 1A***, ***Videos 1, 2, 3***). However, the motions of eGFP-CCR5 particles were heterogeneous (***Figure 2A***). Eighty percent of the pooled CCR5 tracklets were mobile with Brownian motion, while 20 % were classified as restricted motion (i.e. immobile and confined) (***Figure 2A***). We observed almost no directed trajectories (< 0.5 %). Around fifty percent of particles (52 %) exhibited Brownian motion over the entire length of the path (***Figure 2B***). The other half fluctuated between Brownian and restricted motion (***Figure 2B***). This high degree of fluctuation between motions within one trajectory suggested the existence of transient conformations of CCR5 at the plasma membrane.

Together, these analyses revealed heterogeneity of CCR5 motion at the basal state consistent with the diversity of CCR5 forms described previously by other methods (Abrol et al., 2014; Colin et al., 2013; Fox et al., 2015; Jin et al., 2018; Scurci et al., 2021).

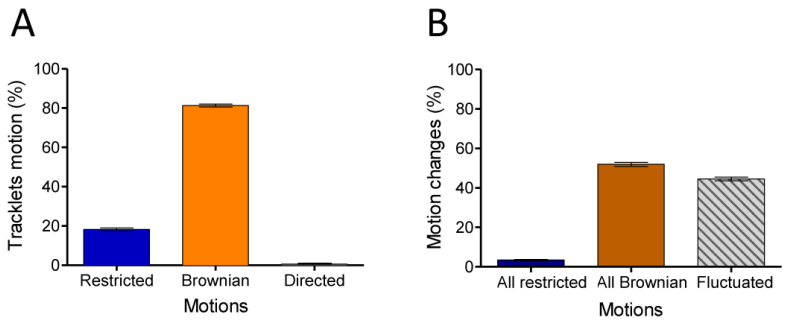

Figure 2. In the basal state, CCR5 exhibits different motions at the plasma membrane. (A) Distribution of tracklets motion: restricted, Brownian, or directed (mean ± SEM, n= 28 305 tracks from 19 cells, 3 independent experiments). (B) Distribution of tracklets motion changes along tracks (mean ± SEM, n= 48 237 tracks from 45 cells, 7 experiments).

Multiple ligands impact CCR5 mobility differently

Since ligands modulate the conformation of CCR5 (Colin et al., 2018; Jacquemard et al., 2021; Jin et al., 2018), we investigated the impact of ligand binding on its spatiotemporal dynamic properties. We evaluated the effect of saturating concentration of ligands (two agonists with different efficacies and the inverse agonist MVC, i.e. a ligand with a negative efficacy) on CCR5 trajectories at the plasma membrane over time. We first incubated the cells in the presence of the native chemokine CCL4 at a saturating concentration (> 100 nM, kd = 0.4 nM) (Colin et al., 2013) for the indicated time. The mobility of the receptor was then assessed immediately after addition of the ligand in a window of 1 to 12 min (***Figure 3A***). CCL4 triggered no significant change in CCR5 mobility after 10 min of stimulation (***Figure 3B***). However, a longer time of CCL4 stimulation (> 12 min) increased the percentage of restricted CCR5 tracklets, indicating localized immobility of a small fraction of receptors (***Figure 3-figure supplement 1***). We also noted the formation of large and immobile spots after 12 min of stimulation (***Video 4***).

We compared the effect of CCL4 with that of an agonist targeting a greater proportion of receptor conformations and displaying a greater agonist efficacy, PSC-RANTES (Escola et al., 2010; Jin et al., 2014). We incubated the cells in the presence of a saturating concentration of PSC-RANTES (20 nM, Ki = 1.9 nM) (Colin et al., 2013) and evaluated the motion of the receptors under the same conditions. PSC-RANTES triggered a progressive increase in the number of tracklets classified as restricted motion over time (***Figure 3A***). Ten minutes after stimulation with PSC-RANTES, about 50 % of eGFP-CCR5 tracklets were in a restricted state (46 %) against 17 % under basal conditions (***Figure 3B***). Consequently, the fraction of all Brownian trajectories decreased, while the fraction of fluctuated and all restricted trajectories increased (***Figure 3C***). Simultaneously, we observed the formation of large immobile spots (5 to 10 per cell) in PSC-RANTES-treated cells (***Figure 3D, left***). These large spots had a long lifespan (50 to 100 frames) (***Video 5***). The quantification of the fluorescence intensity of the spots from the frame 1 of live-imaging movies showed that the large spots had, on average, intensity 4 times higher than the other spots, indicating a clustering of at least 4 receptors per large spot (***Figure 3D, right***). These results revealed a change in CCR5 mobility upon activation towards receptor immobilization and clustering, supporting receptors trapping in nanodomains.

Unlike agonists, the inverse agonist MVC (10 µM, Kd = 1 nM) did not restrict receptor mobility (***Figure 3A, B, C***). On the contrary, the fraction of restricted eGFP-CCR5 tracklets at the surface of MVC-treated cells showed a slight decrease compared to untreated cells (***Figure 3B***). We verified the specificity of PSC-RANTES-induced CCR5 immobility by treating cells with MVC before PSC-RANTES stimulation. MVC treatment impaired PSC-RANTES-induced receptor immobilization (***Figure 3E-F***), indicating that CCR5 immobilization depended on PSC-RANTES binding to CCR5.

These results showed that distinct ligands differently stabilize CCR5 in living cells, in accordance with our previous results (Colin et al., 2013; Colin et al., 2018; Jin et al., 2014; Jin et al., 2018). Interestingly, the amount of receptors immobilized correlates with the efficacy of ligands (PSC-RANTES > CCL4 > MVC), suggesting a link between receptor activation and immobilization.

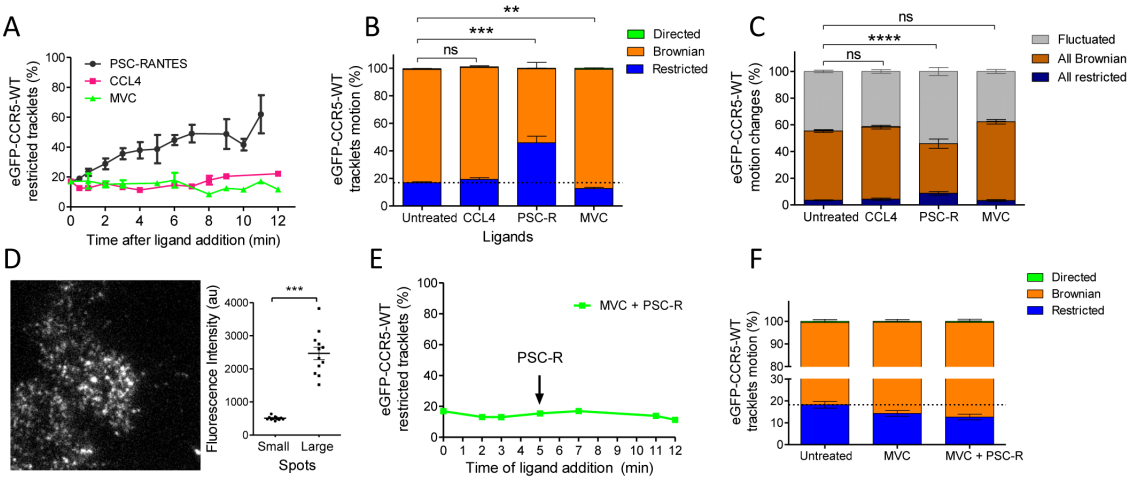

Figure 3. Different ligands, agonists and inverse agonist, impact CCR5 mobility differently. eGFP-CCR5-WT expressing cells were treated or not with a saturating concentration of agonists (CCL4, 200 nM or PSC-RANTES, 20 nM) or inverse agonist (maraviroc, 10 μM) and single particle tracking analysis was performed. (A) Percentage of restricted tracklets after treatment over time (n= tracks from 10, 4, and 3 cells for PSC-RANTES, CCL4, and MVC conditions respectively, at least 3 independent experiments). (B) Distribution of tracklets motion after 10 min of treatment (mean ± SEM, n= 40 564, 15 421, 11 213, 9 828 tracks for each condition from 38, 14, 12, 9 cells respectively, at least 3 independent experiments). Unpaired t test on restricted motions only: ns, nonsignificant; ***P ≤ 0.005; ***P ≤ 0.0001*. (C) Distribution of tracklets motion changes along tracks after 10 min of treatment (mean ± SEM, n= 48 237, 8 954, 16 668, 9 828 tracks from 45, 9, 17, 9 cells for each condition, at least 3 experiments). Unpaired t test on all restricted motions only: ns, nonsignificant; *****P ≤ 0.0001*. (D) (Left) Single particle detection of eGFP-CCR5-WT after 3 min of stimulation with PSC-RANTES (20 nM) from frame 1 of live-imaging movie (one representative image). (Right) Mean of the sum of fluorescence intensity under large immobile spots and small mobile spots after 3 to 10 min of stimulation (mean ± SEM, n= at least 40 spots from 12 cells, 3 experiments). (E) Percentage of restricted tracklets after successive stimulation

with maraviroc (10 μM, 5 min) and PSC-RANTES (20 nM, 5 to 12 min) (one representative experiment). (F) Distribution of tracklets motions after successive stimulation with maraviroc (10 μM, during 5 min) and PSC-RANTES (20 nM, during 6 min) (mean ± SEM, n= 14 467, 3 601, 2 075 tracks from 14, 2, 2 cells respectively, 1 experiment).

Figure supplement 1. Effect of CCL4 on CCR5 mobility.

Video 4. TIRF movie acquired at 30 Hz of a cell stably expressing eGFP-CCR5-WT and treated by CCL4 (100 nM) for 14 min.

Video 5. TIRF movie acquired at 30 Hz of cells stably expressing eGFP-CCR5-WT and treated by PSC-RANTES (20 nM) for 3 min.

Gi coupling and β-arrestin association influence CCR5 motion differently under basal state and stimulated conditions

To further address the above hypothesis, we sought to determine whether the mobility of CCR5 is influenced by its coupling to Gi protein, which stabilizes the receptor in an activated state. We analyzed the pool of restricted CCR5 tracklets in the presence of pertussis toxin (PTX), which uncouples the receptor from Gi proteins (***Figure 4A***).

In the basal state, the fraction of restricted eGFP-CCR5 tracklets from cells pre-treated with PTX decreased compared to untreated cells (***Figure 4A***). Under this condition, PTX also inhibited chemotaxis, a process that depends on CCR5 coupling to Gi proteins (***Figure 4*-figure supplement 1)**. These results thus suggested that a small subset of CCR5 is in a Gi protein-bound form in its basal state, which may contribute to the transient restriction of the motion of CCR5 at the cell surface.

After stimulation, receptor immobilization could be due to the recruitment of receptors in hub areas where the receptor meets the activation machinery and in particular the G protein (Sungkaworn et al., 2017). To evaluate the role of Gi coupling on receptor immobilization after PSC-RANTES stimulation, we analyzed tracks of TIRF movies of PSC-RANTES-stimulated cells pretreated or not with PTX. In this condition, the fraction of restricted tracklets increased over time after stimulation in the same proportion

304 regardless of PTX treatment (***Figure 4B***). This suggested that Gi coupling was not
305 involved in PSC-RANTES dependent immobilization of CCR5 after several minutes of
306 stimulation. This result is actually consistent with our previous study showing high affinity
307 interaction of PSC-RANTES with Gi protein uncoupled CCR5 (Colin et al., 2013).

308 After stimulation by PSC-RANTES, CCR5 follows a clathrin-dependent endocytosis
309 pathway, involving β-arrestins, which bridge the receptor to AP2 and clathrin (Delhaye et
310 al., 2007; Jin et al., 2014). We previously showed that silencing β-arrestin 1 and β-
311 arrestin 2 endogeneous expressions with siRNA decreased CCR5 internalization after
312 PSC-RANTES stimulation (Jin et al., 2014). Silencing β-arrestins in eGFP-CCR5 cells
313 with siRNA did not impact eGFP-CCR5 motion in the basal state (***Figure 4C***) but
314 inhibited PSC-RANTES-induced eGFP-CCR5 immobilization and clustering (***Figure 4D***).
315 These experiments indicated that β-arrestins contributed to CCR5 immobilization after
316 stimulation.

317 Together, these results pointed to the existence of a fraction of CCR5 in a transient pre-
318 assembled signaling complex in the basal state, which is consistent with previous
319 studies showing CCR5 constitutive activity (Garcia-Perez et al., 2011; Lagane et al.,
320 2005). They also suggested that the fate of CCR5 several minutes after activation is
321 independent of Gi coupling but dependent on β-arrestin recruitment, in accordance with
322 receptor desensitization and uncoupling after activation (Flanagan, 2014).

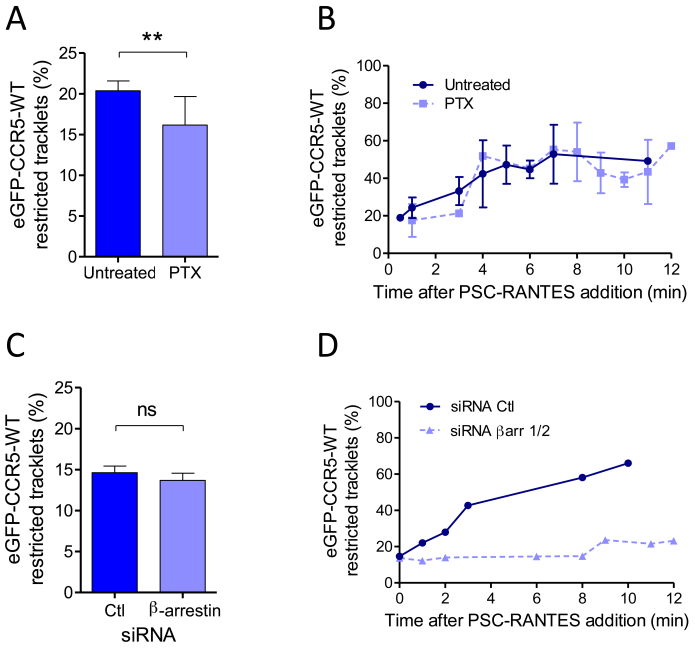

323

324 **Figure 4.** Gi coupling and β-arrestins association restrict CCR5 mobility at basal state or after
325 PSC-RANTES stimulation. (A) Percentage of restricted tracklets in eGFP-CCR5-WT expressing
326 HEK 293 cells pre-treated or not with 100 ng/ml of PTX for 3 h (mean ± SEM, n= 8 614 and 11
327 377 tracks for each condition, 12 and 15 cells respectively, 3 independent experiments). Unpaired
328 t test: p value 0.0083**. (B) Percentage of restricted tracklets over time of eGFP-CCR5-WT
329 expressed on PSC-RANTES (20 nM) treated cells after incubation or not with PTX (100 ng/ml)
330 (mean ± SD, n= 3 independent experiments). (C) Proportion of restricted tracklets in eGFP-
331 CCR5-WT expressing cells transfected with siRNA βarr1/2 (mean ± SD, n= 6 754 and 8 854
332 tracks for each condition, from 7 and 8 cells respectively). Unpaired t test: p value 0.46, ns. (D)
333 Percentage of restricted tracklets over time of eGFP-CCR5-WT expressed on PSC-RANTES (20
334 nM) treated cells after siRNA βarr 1/2 transfection (n= 1 representative experiment).

335 **Figure supplement 1.** Effect of PTX treatment on chemokine-mediated chemotaxis.

336

337 ## Immobilization of CCR5 after stimulation depends on its oligomeric state

338 We previously showed by energy transfer experiments that a point mutation of CCR5 in
339 TM5 (L196K) leads to a receptor, which has a reduced dimerization capacity compared
340 to CCR5-WT (Jin et al., 2018). To study the role of CCR5 dimerization on its mobility, we

generated HEK 293 cells stably expressing eGFP-CCR5-L196K in the same proportion to the clone expressing eGFP-CCR5-WT.

We studied the molecular composition of both eGFP-CCR5-L196K and eGFP-CCR5-WT in these cells by analyzing the fluorescence intensity of eGFP per spot from the frame 1 of live-imaging movies. In a previous study, we calibrated the fluorescence intensity of eGFP while spotted on glass coverslip (Salavessa et al., 2021). We showed that most of eGFP spots bleached in a single step, suggesting that eGFP corresponds to 1 molecule, with an average fluorescence intensity of 300-500 au (Salavessa et al., 2021). In eGFP-CCR5 expressing cells, the fluorescence intensities were distributed in Gaussians, which we classified with the Akaike information criterion (AIC, see Material and Methods) (Akaike, 1974). We observed three types of Gaussians with double or triple mean intensities (300, 600, 900 au), which likely correspond to spots comprising 1, 2, or 3 receptors (***Figure 5A***). This reflected the existence of a heterogeneous distribution of receptors. In this classification, the WT receptor distributed in 50 % monomers, 40 % dimers, and 10 % oligomers (trimers or more) at the plasma membrane, while eGFP-CCR5-L196K was mostly in a monomeric form (75 % monomers, 25 % dimers) (***Figure 5B***). These results revealed that eGFP-CCR5-L196K was mostly monomeric at the surface of living cells and that the fusion of eGFP to CCR5 did not alter the effect of L196K mutation on CCR5 dimerization.

In the presence of MVC, both eGFP-CCR5-WT and eGFP-CCR5-L196K distribution exhibited 50 % monomers, 40 % dimers, and 10 % oligomers (***Figure 5B***). The change of eGFP-CCR5-L196K stoichiometry distribution in the presence of MVC confirmed our previous results showing that MVC stabilized CCR5 in a novel dimeric form, which was not disrupted by the introduction of a lysine in TM5 (Jin et al., 2018).

To investigate the impact of CCR5 dimerization on its mobility, we compared the motion of eGFP-CCR5-L196K to eGFP-CCR5-WT at the cell surface. As for eGFP-CCR5-WT, eGFP-CCR5-L196K tracklets were predominantly classified as Brownian tracklets motion (85 % of the tracklet motions are Brownian), suggesting that monomeric and dimeric forms of CCR5 exhibited similar behavior at the surface of cells in the basal state (***Figure 5C***). However, we observed a decrease in the proportion of restricted tracklets for eGFP-CCR5-L196K compared to eGFP-CCR5-WT (***Figure 5C***). These data suggested that dimerization contributed to the stability of CCR5 molecules at the cell surface, as previously proposed (Calebiro et al., 2013).

To test whether eGFP-CCR5-L196K coupling to Gi protein accounts in its restriction as shown for eGFP-CCR5-WT, we pre-treated cells with PTX. Contrary to eGFP-CCR5-WT, PTX treatment did not alter the proportion of the eGFP-CCR5-L196K restricted tracklets pool (***Figure 5D***), suggesting that most of eGFP-CCR5-L196K were not precoupled to the Gi protein at the basal state or that G protein precoupling induces differential effects on the dynamics of both receptors. Supporting the first hypothesis, previous biochemical and energy transfer experiments on a distinct GPCR showed that there could be a link between dimerization and Gi coupling at basal state (Maurice et al., 2010).

To investigate whether dimerization affected CCR5 mobility after stimulation, we analyzed single-molecule movies of eGFP-CCR5-L196K cells after PSC-RANTES treatment (***Figure 5E-F***). Contrary to eGFP-CCR5-WT massive immobilization and clustering upon PSC-RANTES treatment (***Figure 3A-B***), eGFP-CCR5-L196K was only slightly immobilized after 10 minutes of treatment (***Figure 5E-F***), while large immobile spots were not detected (***Video 6***). This result indicated that CCR5 immobilization and clustering after stimulation depend on CCR5 dimerization.

Because CCR5-WT immobilization involved β-arrestins (***Figure 4D***), an explanation for the lack of PSC-RANTES induced eGFP-CCR5-L196K immobilization is that eGFP-CCR5-L196K fails to recruit β-arrestins and therefore, is not desensitized and/or internalized after stimulation. To test this hypothesis, we evaluated PSC-RANTES-induced internalization of the dimerization-compromised mutant compared to the WT receptor in feeding experiments using FLAG-SNAP-CCR5 expressing cells (Delhaye et al., 2007; Jin et al., 2018). A saturating concentration of PSC-RANTES decreased cell surface expression of both receptors, but not in the same proportion (***Figure 5G***), suggesting that CCR5 dimerization impacted its internalization process. However, while eGFP-CCR5-L196K immobilization was drastically impaired, its internalization was not fully abrogated. These results supported that dimerization is a pre-requisite to the immobilization of the receptor, but was not essential for receptor internalization. This ruled out a necessary step of massive receptor immobilization before internalization and revealed that different mechanisms may contribute to CCR5 internalization depending on the receptor conformation.

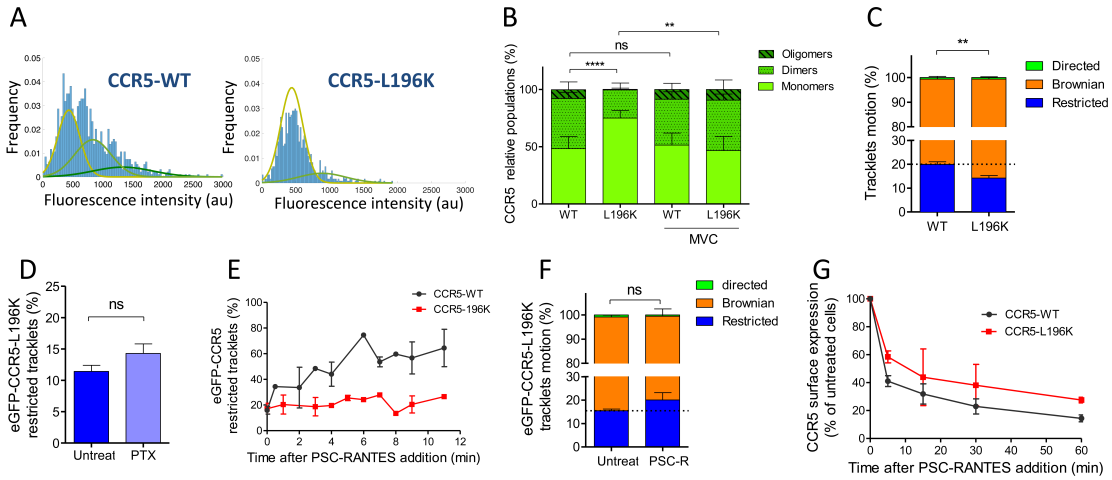

Figure 5. Dimerization through TM5 alters CCR5 mobility and trafficking. (A) Distribution of the fluorescence intensity of spots detected at the surface of HEK 293 cells expressing eGFP-CCR5-

WT or eGFP-CCR5-L196K. One representative experiment out of 6 (n= 943 spots from 6 cells and 1 207 spots from 8 cells for each condition); (B) Quantification of the fluorescent populations depending on the mean of the gaussian at the surface of cells treated or not with MVC (10 μM) (mean ± SD, nWT = 5 171 spots from 47 cells, 9 experiments; nL196K = 3 144 spots from 30 cells, 5 experiments; nWT-MVC = 3 055 spots from 25 cells, 4 experiments; nL196K-MVC = 1 776 spots from 16 cells, 3 experiments). Unpaired t test on monomers: p value $**P \leq 0.005$; $****P \leq 0.0001$; ns $P \geq 0.05$; (C) Distribution of pooled trackets motion of eGFP-CCR5-WT and eGFP-CCR5-L196K (mean ± SEM, n = 11 321 tracks from 10 cells and 10 460 tracks from 12 cells in each condition; 2 independent experiments). Unpaired t test on the restricted tracklets: p value 0.0015**. (D) Percentage of restricted tracklets in eGFP-CCR5-L196K cells pre-treated or not with 100 ng/ml of PTX for 3 h (mean ± SEM, n= 7 cells). Unpaired t test: p value 0.15, ns. (E) Percentage of restricted tracklets over time of PSC-RANTES induced eGFP-CCR5-WT or eGFP-CCR5-L196K expressing cells (mean ± SD of 3 independent experiments). (F) Distribution of tracklets motion after 10 min of PSC-RANTES stimulation (20 nM) (mean ± SEM, n= 11 218 tracks from 10 cells and 5 433 tracks from 4 cells for untreated and PSC-RANTES treated cells respectively, 2 independent experiments). Unpaired t test: p value 0.055, ns. (G) CCR5 internalization. Cell surface expression of FLAG-SNAP-CCR5-WT or FLAG-SNAP-CCR5-L196K was monitored by flow cytometry in stable HEK 293 cell clones after stimulation with a saturating concentration of PSC-RANTES (20 nM) for the indicated time. The percentage of total bound anti-FLAG antibody was calculated from the mean fluorescence intensity relative to untreated cells (mean ± SD from two independent experiments).

Video 6. TIRF movie acquired at 30 Hz of a cell stably expressing eGFP-CCR5-L196K and treated by PSC-RANTES (20 nM) for 2 min.

Distinct HIV-1 envelope glycoproteins gp120 differently influenced CCR5 dynamics

Pharmacological studies suggested that distinct CCR5 conformations at the cell surface differentially engaged distinct HIV-1 envelope glycoproteins gp120 (Colin et al., 2018). Since we showed here that CCR5 mobility and ligand engagement are intrinsically linked, we used our mobility classification method to characterize the effect of different HIV-1 gp120s on CCR5 mobility and tested in living cells whether different gp120s engaged different conformational states of CCR5.

We tested the effect of two soluble gp120s, gp #25 and gp #34, described to induce distinct conformational rearrangements in CCR5 (Jacquemard et al., 2021), and to have different binding capacities to the receptor and fusogenic efficacies (Colin et al., 2018). Twenty min of gp120s exposure slightly modulated the mobility of eGFP-CCR5-WT, although this trend was not statistically significant (***Figure 6A, C***). However, and in contrast to what we observed using chemokines as ligands, the HIV-1 gp120s immobilized eGFP-CCR5-L196K, with gp #34 having the highest effect (***Figure 6B, C***). This suggested (i) that gp120s stabilized CCR5 conformations, which were different from those stabilized by chemokines, and (ii) that different envelopes also stabilized differently CCR5 conformations, in accordance with our previous result (Colin et al., 2013; Colin et al., 2018).

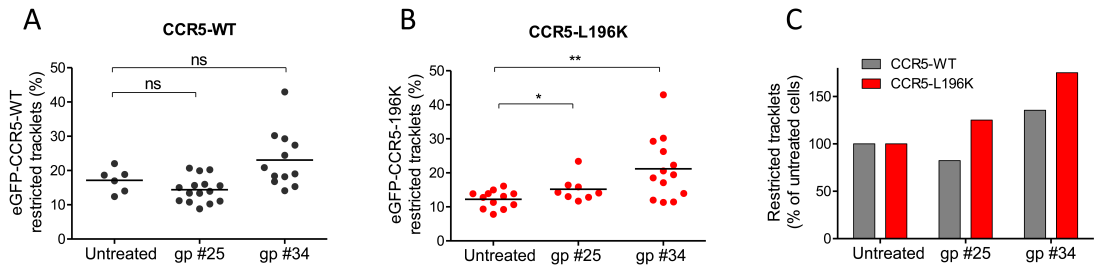

Figure 6. HIV-1 gp120s binding restricts CCR5 mobility. Soluble gp120s were incubated 30 min at RT in the presence of soluble CD4 (ratio sCD4/gp120 >5) to allow their binding to CCR5. Then, gp120-sCD4 complexes were added to live eGFP-CCR5-WT or eGFP-CCR5-L196K expressing cells during at least 20 min before single particle analysis. The proportion of restricted tracklets after gp #25 and gp #34 treatment (100 nM) (in complex with sCD4) on eGFP-CCR5-WT (A, C) or eGFP-CCR5-L196K (B, C) expressing cells was represented (n=3 independent experiments). Unpaired t test: $^{**}P \leq 0.005$; $^{***}P \leq 0.0001$; ns $P \geq 0.05$.

Discussion

In this study, we developed a statistical method to classify the motion of fluorescent particles at the cell surface. We applied this method to track eGFP-CCR5 under different stimuli and different conformations. We showed that the receptor fluctuates between Brownian and restricted motions at the cell surface, depending on (1) precoupling to Gi proteins at the basal state; (2) the type of ligand bound to the receptor, and in particular its efficacy on receptor activation and interaction with β-arrestins; and (3) receptor dimerization. Indeed, CCR5 mobility changes following agonist stimulation were dependent on β-arrestins recruitment and receptor dimerization, but were independent of receptor interaction with Gi proteins. This study demonstrated that coupling single molecule tracking to a statistical classification of trajectories is a powerful approach to characterize the dynamic behaviors of functionally different receptor populations at the plasma membrane.

Diversity of ligand-free forms of CCR5 at the cell surface.

Quantitative analysis of the motion of CCR5 particles and their numbering within the fluorescent spots present at the cell membrane of HEK 293 cells revealed in the basal state (i) two classes of receptor trajectories, Brownian (80 %) and restricted (20 %) (***Figure 2***) and (ii) different oligomeric states (***Figure 5***): monomers (50 %), dimers (40 %), and oligomers (more than three receptors) (10 %). These features shared with other GPCRs (Gormal et al., 2020; Martinez-Munoz et al., 2018; Sungkaworn et al., 2017; Tabor et al., 2016; Veya et al., 2015), established the existence of multiple CCR5 forms at the cell membrane.

In addition, our statistical method highlighted a fluctuation between Brownian and restricted states during the same trajectory, suggesting the existence of transient populations of receptors (***Figure 2B***). The change in mobility between periods of

confinement separated by free diffusion could be attributed to the molecular organization of the receptor oscillating between different oligomeric forms at the cell surface (monomers, dimers, oligomers), as proposed for CCR5 (Jin et al., 2018) or other receptors (Isbilir et al., 2020; Kasai et al., 2018; Martinez-Munoz et al., 2018; Tabor et al., 2016). In agreement with this, we observed differences in mobility between monomers and dimers of CCR5 (***Figure 5C***). Change in mobility could also be linked to a transient coupling to G proteins, leading to a transient immobility of the receptor in the basal state. This hypothesis is supported by our data in the presence of PTX (***Figure 4A***) or in the presence of the inverse agonist MVC (***Figure 3A, B***), which both uncouple the receptor from G proteins and decreased the proportion of immobile receptors. These data are consistent with dual-color TIRF-M analysis of adrenergic receptor and G protein, showing that an active receptor-G protein complex is formed in a confined region of the plasma membrane at the basal state and lasts around 1 second (Sungkaworn et al., 2017). However, they contrast with a study on mGluR3 showing higher mobility of the receptor when complexed with G protein (Yanagawa et al., 2018). This suggested that dynamics of distinct GPCRs can be differently impacted by coupling to G proteins. Regarding β-arrestin association, we showed using siRNA that CCR5 was not precoupled to β-arrestins in its basal state (***Figure 4C***). This result suggests that CCR5 conformations, which bind to G proteins are not recognized by β-arrestins. This is consistent with the idea that the conformations of receptors interacting with G proteins and β-arrestins are different (Lagane et al., 2005).

Different ligands recognize/stabilize different sets of CCR5.

We showed that CCR5 mobility is influenced differently according to the ligand it binds. Chemokine-induced activation of eGFP-CCR5-WT decreased mobility and leads to clustering (***Figure 3B, D***), effects not observed with the inverse agonist MVC and

abolished by MVC (***Figure 3A, B and Figure 3E, F***). This result reinforces the link between GPCR mobility and ligand binding proposed for GPCRs of different classes (Gormal et al., 2020; Moller et al., 2020; Veya et al., 2015; Yanagawa et al., 2018).

We also showed that two agonists targeting different amount of receptors (CCL4 and PSC-RANTES) (***Figure 3***) restricted receptor motion in a different proportion, leading to speculate a relationship between mobility restriction and quantity of targeted receptor, the greater the number of receptors targeted, the more receptors immobilized and trapped. Although other possibilities should be considered, such as the dynamic nature of the ligand-bound conformations, we proposed that characterizing ligands by their impact on receptor motion opens a new way to classify biased ligands.

Applied to viral envelope glycoproteins, our single-particle approach revealed that HIV-1 gp120s displayed an agonist-like influence on CCR5 mobility, albeit to different extent according to the nature of the gp120 (***Figure 6***). This feature contrasts with the cryo-EM structure of the CD4-gp120-CCR5 complex, showing that CCR5 adopts inactive confomation (Shaik et al., 2019). However, it is in line with gp120s-induced CCR5 signaling (Brelot & Chakrabarti, 2018; Flanagan, 2014) and with recent MD simulations showing that gp120 binding reorients characteric microswitches involved in GPCR activation (Jacquemard et al., 2021). The fact that the fraction of immobilized receptors varied between gp120s could reflect that they do not bind to the same CCR5 conformations, as previously shown (Colin et al., 2018; Jacquemard et al., 2021), and suggests that these gp120s behave themselves as biased agonists. These features of gp120s will help understand the determinants of HIV-1 tropism.

Single particle tracking analysis revealed that dimerization regulates the fate of activated CCR5.

Our results suggest that receptor dimerization may regulate precoupling of CCR5 to Gi proteins. Indeed, the mobility of the dimerization-compromized mutant eGFP-CCR5-L196K was not affected by PTX treatment, in contrast to the WT receptor (***Figure 4A and Figure 5D***). This suggests that most eGFP-CCR5-L196K receptors that reside preferentially as monomers are not coupled to Gi proteins in the basal state, in agreement with previous conclusion on CXCR4 (Isbilir et al., 2020). Alternatively, but not exclusively, CCR5-L196K dimers might also be impaired in their ability to be precoupled to Gi proteins, contrary to WT receptor dimers.

Our analysis suggests that dimerization is a pre-requisite to receptor immobilization and clustering upon activation by chemokine agonists. Indeed, unlike eGFP-CCR5-WT, eGFP-CCR5-L196K receptors are only marginally immobilized in the presence of PSC-RANTES (***Figure 5E***). This result is not due to impaired binding of the chemokine, because we controlled that PSC-RANTES induced efficient endocytosis of the mutant receptor (***Figure 5G***). Receptor immobility and clustering were independent of Gi protein coupling, as exemplified by unaffected CCR5 mobility after 10 min of agonist stimulation in PTX pre-treated cells (***Figure 4B***), but most likely related to uncoupled and desensitized form of CCR5 that accumulate in CCS (clathrin-coated structures), as proposed (Grove et al., 2014; Yanagawa et al., 2018). This hypothesis was strengthened with the essential role of β-arrestins in activated receptor immobility and clustering (***Figure 4D***). We cannot rule out that activated receptor clustering may in addition correspond to an accumulation of receptor in early endosome for a second phase of activation (Irannejad et al., 2013).

In line with this, we showed that dimerization regulates endocytosis (***Figure 5G***). The lack of immobilization of the dimerization-compromised mutant leads to a suboptimal internalization of the receptor. This could be due to the impact of dimerization on the route of endocytosis (dependent or independent of CCS) or on the association of β-arrestins with the receptor, which stability regulates the fate of the receptor (Bonsch et al., 2015). This later hypothesis is in accordance with studies showing an impact of dimerization on β-arrestins recruitment (Fillion et al., 2019). Differential effects of gp120 on immobilization of CCR5 WT and L196K (***Figure 6***), compared to chemokines (***Figure 5***), could also be explained by differences in recruitment of β-arrestins, linked to differences in the stabilized conformations of receptors.

Finally, our study suggested that CCR5 can be activated whether monomeric or dimeric. We showed that eGFP-CCR5-L196K, while mostly monomeric in its basal state (***Figure 5B***), is still internalized (***Figure 5G***), suggesting that monomers can be activated, which is consistent with studies reporting that GPCR monomers can be active enough on their own to be functional (Whorton et al., 2007).

In summary, our single-particle tracking analysis established that a diversity of CCR5 forms exists at the surface of living cells and that distinct ligands stabilize different receptors. This approach also revealed that receptor dimerization is involved in Gi protein-coupling in the basal state, and in the immobilization of receptors after activation, pointing out that receptor conformation regulates GPCRs signaling and fate after activation. In addition, our work suggested that the different receptor conformations likely engaged different ways of regulation, expanding GPCRs functions.

Materials and Methods

Cell culture and reagents

The HEK 293 cells stably expressing SNAP-FLAG-CCR5-WT and SNAP-FLAG-L196K and the A3.01 human T cell line stably expressing CCR5 (A3.01-R5) were previously described (Colin et al., 2013; Jin et al., 2018). These cell lines were maintained in Dubelcco's modified Eagle medium (DMEM) (Thermo Fisher Scientific) or RPMI 1640 medium supplemented with 10 % Fetal Bovine Serum (FBS, GE Healthcare) and 100 µg/ml penicillin/streptomycin (Life technologies).

The CCR5 inverse agonist maraviroc (MVC) was obtained from the National Institutes of Health. The native chemokine CCL4 was chemically synthetized by F. Baleux (Institut Pasteur, Paris, France). The chemokine analog PSC-RANTES (N-α-(n-nonanoyl)-des-Ser(1)-[L-thioprolyl(2), L cyclohexylglycyl(3)] RANTES(4-68)) was obtained through the Center for Aids reagents, National Institute for Biological Standards and Control (NIBSC, UK). The primary antibodies used are the anti-GFP (Roche), the anti-CCR5 2D7 mAb (BD-Biosciences); the anti-FLAG monoclonal antibodies M1 or M2 (Sigma-Aldrich). Secondary antibodies used were a phycoerythrin (PE)-conjugated anti-mouse antibody (BD Biosciences). The toxin from Bordetella pertussis (PTX) used at a 100 ng/ml concentration were from Sigma. The βarr1/2 siRNA (5'-ACCUGCGCCUUCCGCUAUG-3') and a scrambled siRNA (control, 5'-UGGUUUACAUGUCGACUAA-3') (Dharmacon) were transfected by RNAimax (Invitrogen) according to the instructions of the manufacturer, as described (Jin et al., 2014). To select siRNA positive cells, cells were co-transfected with a plasmid coding the fluorescent protein mcherry (gift of F. Perez, Institut Curie). Soluble, monomeric HIV-1 glycoprotein gp120 was produced using a semliki forest virus (SFV) system as described (Benureau et al., 2016; Colin et al., 2018). The sequence coding for gp120 #25 and gp120 #34 were from PBMCs of

607 patients collected early after seroconversion or in the AIDS stage of infection,
608 respectively (Colin et al., 2018). Recombinant soluble CD4 (sCD4), produced in S2 cell
609 lines, was purified on a strep-Tactin column using the One-STrEP-tag fused to the CD4
610 C-tail as a bait (production and purification of recombinant proteins technological
611 platform, C2RT, Institut Pasteur).

612 ### Generation of cell lines

613 The eGFP-CCR5 plasmid was a gift of F. Perez (Institut Curie, Paris, France)
614 (Boncompain et al., 2019). The mutant eGFP-CCR5-L196K (substitution of L196 with a
615 lysine) was generated by site-directed mutagenesis using the QuickChange II
616 Mutageneis kit (Agilent Technologies) according to the manufacturer's instruction. This
617 mutant was verified by sequencing (Eurofins). HEK 293 cells stably expressing eGFP-
618 CCR5-WT and HEK 293 cells stably expressing eGFP-CCR5-L196K were generated by
619 calcium phosphate transfection and cultured for several weeks in 1 mg/ml G418
620 (Geneticin, Invitrogen). Cell Clones were screened and sorted by flow cytometry (Attune
621 NxT flow cytometer, Thermo Fisher) using an anti-GFP monoclonal antibody.

622 ### Receptor cell surface expression levels and internalization measured by flow cytometry

623 Flow cytometry was used to quantitate the internalization of FLAG-SNAP-CCR5-WT
624 compared to FLAG-SNAP-CCR5-L196K stably expressed in HEK 293 cells (Delhaye et
625 al., 2007; Jin et al., 2018). We measured the levels of cell surface CCR5 stained with the
626 anti-FLAG M2 antibody and with an anti-mouse coupled to phycoerythrin (PE) after
627 chemokine treatment or not. Cells were incubated with a saturable amount of M2 for 45
628 min to labels receptors present at the plasma membrane, then incubated in the presence
629 (or not) of 20 nM PSC-RANTES for the indicated time at 37°C. Cells were chilled to 4°C
630 and stained with a PE conjugated anti-mouse IgG. Mean values were used to compute
631 the proportion of internalized receptors as indicated by a decrease of immune-reactive

surface with PSC-RANTES compared with untreated cells. Cells were analyzed with Attune NxT flow cytometer (Thermo Fisher). At least 5,000 cells were analyzed per experiment using Kaluza software. Background was subtracted using the fluorescence intensity obtained on the parental HEK 293 cells.

Chemotaxis

CCR5 expressing A3.01 cells (A3.01-R5, 1.5 X 10^5), pre-treated or not with PTX (100 ng/ml) during 3 h, in prewarmed RPMI-1640 supplemented with 20 mM Hepes and 1% serum, were added to the upper chambers of HTS-Transwell-96 Well Permeable Supports with polycarbonate membrane of 5 µm pore size (Corning). PSC-RANTES (33.7 nM) or SDF-1 (control, 10 nM) was added to the lower chambers. Chemotaxis proceeded for 4 h at 37 °C in humidified air with 5% CO2. The number of cells migrating across the polycarbonate membrane was assessed by flow cytometry with Attune NxT flow cytometer (Thermo Fisher). Specific migration was calculated by subtracting spontaneous migration from the number of cells that migrated toward the chemokine.

Live cell TIRF imaging

Round 25 mm No. 01 glass coverslips (Fisher Scientific) were pre-cleaned with 70% ethanol followed by acetone, with three consecutive washes in ddH2O. 1.15 × 10^5 cells were plated onto pre-cleaned coverslips 72 h before imaging. Cells were imaged in TIRF medium (25 mM HEPES, 135 mM NaCl, 5 mM KCl, 1.8 mM $CaCl_2$, 0.4 mM $MgCl_2$, 4.5 g/l glucose and 0.5% BSA, pH 7.4). Movies were acquired with an LSM 780 Elyra PS.1 TIRF microscope (Zeiss) equipped with an EMCCD Andor Ixon 887 1K camera, and using an alpha Pin Apo 100x/1.46 oil objective, a 488 nm (100 mW) HR solid laser line, and a BP 495-575 + LP 750 filter to detect eGFP-CCR5. Image acquisition was done at 1 frame / 33 msec (30 Hz) (100 to 200 frames), with 8 % (tracking) or 15 % (stoechiometrie) laser power at 37°C. Approximately 5-10 cells were acquired per

condition, per experiment. All live-imaging movies were analyzed using the open-source software Icy (Institut Pasteur).

Track analysis protocol

Tracking receptors in TIRF imaging with Icy software

To automatically detect eGFP-CCR5 tracks at the plasma membrane upon time, we used the software Icy (http://icy.bioimageanalysis.org) and the plugin *Spot tracking*, which reports their *xy* displacement and intensities, as previously described in Bertot *et al.* (Bertot et al., 2018). *Spot tracking* was set to detect spots with approximately 3 pixels, and a threshold of 135. All other parameters were as default. Tracks were analyzed with the *Track manager* plugin. All data was exported to *Excel* for further analysis.

Tracks containing more than 10 % of virtual detections and more than three successive virtual detections were excluded from the track classification.

Splitting tracks into tracklets

We deal with trajectories that have very different lengths and we want to estimate motion variations along the trajectory. Thus, we split all long tracks into several tracklets in order to better classify local motions. According to Section 1, this is done by setting $\mathrm{N} = 5$ and considering only the tracks with length larger than 6. Then, the different successive tracklets are defined by using the position between the $(5\mathrm{k})^{\mathrm{th}}$ and $(5(\mathrm{k}+1))^{\mathrm{th}}$ frame with $\mathrm{k} \geq 0$.

Detecting immobile receptors

To classify tracklets and identify distinct receptor dynamics, we first identified immobile receptors. In time lapse imaging, a tracklet X is defined by the vector of its successive positions at the different time frames $X = (X_0, \dots, X_{N-1})$, with *N* the length of the tracklet. We considered that a receptor was immobile if

$$\max_{i \neq j = 0,\ldots,N-1} ||X_i - X_j|| < \sqrt{2}\, l$$

where *l* is the size of the object (*l=2* pixels typically). In other words, the previous criterion states that a tracklet is immobile if the maximal distance between two different positions is at most equal to the length of the diagonal of the square of edge *l*.

The 3 types of motion of mobile receptors

To classify the other tracklets corresponding to mobile receptors, we used the statistical method introduced in (Briane et al., 2018), which allows to distinguish three main types of motions:

(i) **Brownian motion**: the object (receptor) evolves freely and its trajectory is denoted by σB_t where σ is called the *diffusion coefficient.* The position of the object X_t at time *t* is given by $X_t = X_0 + \sigma B_t$. Brownian increments σdB_t at each time are independent and normally distributed.

(ii) **Directed motion**: the object is actively transported by a deterministic force, and its motion can be modelled by the following stochastic differential equation:

$$dX_t = \mu dt + \sigma dB_t,$$

where μ is a 2D-vector called *drift* and represents the deterministic force, and σ is the *diffusion coefficient* modelling the random Brownian motion.

(iii) **Confined motion**: the object is confined in a domain or evolves in an open but crowded area. This kind of motion can be modeled by an Ornestein-Uhlenbeck process:

$$dX_t = -\lambda(X_t - \mu)dt + \sigma dB_t.$$

We refer to (Durrett, 2018) for more properties about Brownian motion and stochastic calculus.

Statistical classification of mobile tracklets

The motion classification criterion defined in (Briane et al., 2018) essentially considers the ratio between the maximal distance from the initial point and the length of the tracklets. This can be evaluated by defining the following statistics

$$S(X,N) = \frac{\max_{i=0,\dots,N} \left| X_{t_i} - X_{t_0} \right|}{\left[\frac{1}{2} \sum_{i=1}^{N} |X_{t_i} - X_{t_{i-1}}|^2 \right]^{\frac{1}{2}}}$$

where |.| denotes the 2D-Euclidean norm. The classification is made by using the quantiles of order α and 1-α $(\alpha = 0.05)$ of such a statistic for Brownian tracklets.

These quantiles, denoted by q(α) and q(1-α) respectively, depend on α and N, and can be computed by Monte Carlo simulations (see (Briane et al., 2018)). This essentially consists in simulating a high number of Brownian tracklets, computing their statistics values and then evaluating the quantiles.

Then the tracklet motion is said to be confined if S(X,N)<q(α), directed if S(X,N)>q(1-α), and Brownian otherwise. For N=5 and $\alpha = 0.05$, we obtained q(α)= 0.724 and q(1-α) $= 2.464$.

From local classification of tracklet motion to global analysis of receptors' tracks

The above statistical classifier allows estimating the local motion of each receptor. In a second time, we analyzed the difference of tracklet motions along the same longer receptor track. In particular, we evaluated if a receptor changed its type of motion along its trajectory.

Finally, our statistical framework for classifying tracklets motion provided a two-scales picture of the receptors' dynamic behavior: the classification of tracklets provided a

global estimation of receptors' motion, while the identified changes of receptors' motion along their full trajectories indicated the stability of each receptor's motion.

Stoichiometry analysis

Icy software was used to determine the intensity distribution of eGFP-spots. Spots were detected using the Spot detector wavelet-based algorithm (Olivo-Marin, 2002), and then converted to ROIs with 2 pixels radius. Data was exported to Excel. We observed a multimodal distribution of eGFP spots' intensities, and we decided to use the AIC criterion (Akaike information criterion) (Akaike, 1974) to uncover the number of modes in intensity distribution. Each mode putatively corresponds to a number of molecules. Therefore, statistical characterization of the multimodal distribution of eGFP spots' intensity will help to classify each spot with respect to its mode and, therefore, to its estimated number of molecules.

AIC analysis starts with the modeling of the empirical distribution e(x) of eGFP spots'intensities with a weighted sum of Gaussian laws,

$$e(x) = \sum_{i=1}^{p} \alpha_i N(\mu_i, \sigma_i)$$

where p is the number of Gaussian laws in the mixture, α_i the weight of each law and (μ_i, σ_i) the corresponding mean and variance. For a fixed p, we first searched for the optimal parameters $(\alpha_i^*, \mu_i^*, \sigma_i^*)$, for $i = 1..p$ that maximize the likelihood L of the model to the data:

$$L_p(\alpha_1, \mu_1, \sigma_1, \dots, \alpha_p, \mu_p, \sigma_p) = \prod_{j=1}^{n} \left[\sum_{i=1}^{p} \frac{\alpha_i}{\sqrt{2\pi\sigma_i}} \exp\left(-\frac{(x_j - \mu_i)^2}{2\sigma_i} \right) \right]$$

where $(x_1, x_2, \dots, x_n)$ are the observed eGFP intensities in the considered frame of the time-lapse sequence.

This first step of the AIC analysis provides the calibrated parameters $(\alpha_i^*, \mu_i^*, \sigma_i^*)_{i=1..p}$when fitting a *p*-mixture model to data. Then, we computed the optimal number of modes p^* that would describe the different populations of eGFP spots with respect to their estimated number of molecules by minimizing the AIC:

$$AIC(p) = 2k_p - 2\log(L_p^*)$$

where L_p^* is the maximized likelihood the p-mixture model, and $k_p = 3p - 1$ is the number of free parameters of the *p*-mixture model.

Acknowledgments

We are grateful to Françoise Baleux (Institut Pasteur) and Franck Perez (Institut Curie) for the gifts of chemokines and plasmids. We acknowledge Oliver Hartley (University of Genova) and the Programme EVA Centre for AIDS Reagents for the chemokine derivative PSC-RANTES. We acknowledge Stéphane Petres from the Production and Purification of Recombinant Proteins (PPRP) platform (C2RT, Institut Pasteur) for sCD4 production. We thank Audrey Salles from the Photonic BioImaging (PBI) platform (Imagopole) of Institut Pasteur for microscope maintenance and technical help. We thank Vannary Meas-Yedid Hardy (Institut Pasteur), Stéphane Dallongeville (BioImage Analysis Unit, Institut Pasteur), the Image Analysis Hub (C2RT, Institut Pasteur), and VizionR (Paris) for help with the image and data analysis.

This work was supported by grants from Agence National de Recherche sur le SIDA et les hepatitis virales (ANRS), the French Government's Investissement d'Avenir program, Laboratoire d'excellence "Integrative Biology of Emerging Infectious Diseases' (grant ANR-10-LABX-62-IBEID), INCEPTION (ANR-16-CONV-0005) and France-BioImaging Infrastrusture (ANR-10-INBS-04).

FM was the recipient of ANR-10-LABX-62-IBEID fellowship, G.N. of INCEPTION (ANR-16-CONV-0005) fellowship and P.C. of an ANRS fellowship.

Competing Interests: The authors declare that no competing interests exist.

Author Contributions

Fanny Momboisse, Conceptualization, Methodology, Validation, Formal analysis, Investigation, Writing - original draft preparation;

Giacomo Nardi, Conceptualization, Methodology, Software, Validation, Formal analysis, Writing - original draft preparation;

Philippe Colin, Validation, Formal analysis, Investigation;

Melany Hery, Validation;

Nelia Cordeiro, Validation;

Olivier Schwartz, Resources, Supervision, Funding acquisition;

Nathalie Sauvonnet, Conceptualization, Formal analysis, Resources, Writing - original draft preparation, Funding acquisition;

Fernando Arenzana-Seisdedos, Resources, Supervision, Funding acquisition;

Thibault Lagache, Conceptualization, Methodology, Software, Formal analysis, Data curation, Writing - original draft preparation;

Bernard Lagane, Conceptualization, Formal analysis, Resources, Writing - original draft preparation, Supervision, Funding acquisition;

Jean-Christophe Olivo-Marin, Resources, Supervision, Funding acquisition;

Anne Brelot: Conceptualization, Methodology, Validation, Formal analysis, Investigation, Resources, Data curation, Writing - original draft preparation, Visualization, Supervision, Project administration, Funding acquisition.

List of Figure Supplement

Figure1-figure supplement 1

Figure3-figure supplement 1

Figure4-figure supplement 1

Videos Title

Video 1. TIRF movie of a cell stably expressing eGFP-CCR5-WT acquired at 30 Hz. The region of interest was defined by the green line**.**

Video 2. TIRF movie of the same cell as in video 1 analyzed using the Icy software. Red circles correspond to the detection of bright spots using the *Spot detection* pluggin.

Video 3. TIRF movie of the same cell as in video 1 and 2 analyzed using the Icy software and the *Spot tracking* pluggin. Colored lines correspond to the tracked spots.

Video 4. TIRF movie acquired at 30 Hz of a cell stably expressing eGFP-CCR5-WT and treated by CCL4 (100 nM) for 14 min.

Video 5. TIRF movie acquired at 30 Hz of cells stably expressing eGFP-CCR5-WT and treated by PSC-RANTES (20 nM) for 3 min.

Video 6. TIRF movie acquired at 30 Hz of a cell stably expressing eGFP-CCR5-L196K and treated by PSC-RANTES (20 nM) for 2 min.

References

Abrol, R., Trzaskowski, B., Goddard, W. A., 3rd, Nesterov, A., Olave, I., & Irons, C. (2014). Ligand- and mutation-induced conformational selection in the CCR5 chemokine G protein-coupled receptor. *Proc Natl Acad Sci U S A*, *111*(36), 13040-13045. https://doi.org/10.1073/pnas.1413216111

Ahn, D., Ham, D., & Chung, K. Y. (2021). The conformational transition during G protein-coupled receptor (GPCR) and G protein interaction. *Curr Opin Struct Biol*, *69*, 117-123. https://doi.org/10.1016/j.sbi.2021.03.013

Akaike, H. (1974). A new look at the statistical model identification. *IEEE transactions on automatic control*, *19*(6), 716-723.

Aldinucci, D., Borghese, C., & Casagrande, N. (2020). The CCL5/CCR5 Axis in Cancer Progression. *Cancers (Basel)*, *12*(7). https://doi.org/10.3390/cancers12071765

Alkhatib, G., Combadiere, C., Broder, C. C., Feng, Y., Kennedy, P. E., Murphy, P. M., & Berger, E. A. (1996). CC CKR5: a RANTES, MIP-1α, MIP-1ß receptor as a fusion cofactor for macrophage-tropic HIV-1. *Science*, *272*, 1955-1958.

Benureau, Y., Colin, P., Staropoli, I., Gonzalez, N., Garcia-Perez, J., Alcami, J., . . . Lagane, B. (2016). Guidelines for cloning, expression, purification and functional characterization of primary HIV-1 envelope glycoproteins. *J Virol Methods*, *236*, 184-195. https://doi.org/10.1016/j.jviromet.2016.07.019

Berro, R., Klasse, P. J., Lascano, D., Flegler, A., Nagashima, K. A., Sanders, R. W., . . . Moore, J. P. (2011). Multiple CCR5 conformations on the cell surface are used differentially by human immunodeficiency viruses resistant or sensitive to CCR5 inhibitors. *J Virol*, *85*(16), 8227-8240. https://doi.org/JVI.00767-11 [pii]10.1128/JVI.00767-11

Bertot, L., Grassart, A., Lagache, T., Nardi, G., Basquin, C., Olivo-Marin, J. C., & Sauvonnet, N. (2018). Quantitative and Statistical Study of the Dynamics of Clathrin-Dependent and -Independent Endocytosis Reveal a Differential Role of EndophilinA2. *Cell Rep*, *22*(6), 1574-1588. https://doi.org/10.1016/j.celrep.2018.01.039

Boncompain, G., Herit, F., Tessier, S., Lescure, A., Del Nery, E., Gestraud, P., . . . Perez, F. (2019). Targeting CCR5 trafficking to inhibit HIV-1 infection. *Sci Adv*, *5*(10), eaax0821. https://doi.org/10.1126/sciadv.aax0821

Bonsch, C., Munteanu, M., Rossitto-Borlat, I., Furstenberg, A., & Hartley, O. (2015). Potent Anti-HIV Chemokine Analogs Direct Post-Endocytic Sorting of CCR5. *PLoS One*, *10*(4), e0125396. https://doi.org/10.1371/journal.pone.0125396

Brelot, A., & Chakrabarti, L. A. (2018). CCR5 Revisited: How Mechanisms of HIV Entry Govern AIDS Pathogenesis. *J Mol Biol*, *430*(17), 2557-2589. https://doi.org/10.1016/j.jmb.2018.06.027

Briane, V., Kervrann, C., & Vimond, M. (2018). Statistical analysis of particle trajectories in living cells. *Phys Rev E*, *97*(6-1), 062121. https://doi.org/10.1103/PhysRevE.97.062121

Calebiro, D., Rieken, F., Wagner, J., Sungkaworn, T., Zabel, U., Borzi, A., . . . Lohse, M. J. (2013). Single-molecule analysis of fluorescently labeled G-protein-coupled receptors reveals complexes with distinct dynamics and organization. *Proc Natl Acad Sci U S A*, *110*(2), 743-748. https://doi.org/1205798110 [pii]10.1073/pnas.1205798110

Chenouard, N., Bloch, I., & Olivo-Marin, J. C. (2013). Multiple hypothesis tracking for cluttered biological image sequences. *IEEE Trans Pattern Anal Mach Intell*, *35*(11), 2736-3750. https://doi.org/10.1109/TPAMI.2013.97

Colin, P., Benureau, Y., Staropoli, I., Wang, Y., Gonzalez, N., Alcami, J., . . . Lagane, B. (2013). HIV-1 exploits CCR5 conformational heterogeneity to escape inhibition by chemokines. *Proc Natl Acad Sci U S A*, *110*(23), 9475-9480. https://doi.org/1222205110 [pii]10.1073/pnas.1222205110

Colin, P., Zhou, Z., Staropoli, I., Garcia-Perez, J., Gasser, R., Armani-Tourret, M., . . . Lagane, B. (2018). CCR5 structural plasticity shapes HIV-1 phenotypic properties. *PLoS Pathog*, *14*(12), e1007432. https://doi.org/10.1371/journal.ppat.1007432

de Chaumont, F., Dallongeville, S., Chenouard, N., Herve, N., Pop, S., Provoost, T., . . . Olivo-Marin, J. C. (2012). Icy: an open bioimage informatics platform for extended reproducible research. *Nat Methods*, *9*(7), 690-696. https://doi.org/10.1038/nmeth.2075

Delhaye, M., Gravot, A., Ayinde, D., Niedergang, F., Alizon, M., & Brelot, A. (2007). Identification of a postendocytic sorting sequence in CCR5. *Mol Pharmacol*, *72*(6), 1497-1507. http://www.ncbi.nlm.nih.gov/entrez/query.fcgi?cmd=Retrieve&db=PubMed&dopt=Citation&list_uids=17855654

Deupi, X., & Kobilka, B. K. (2010). Energy landscapes as a tool to integrate GPCR structure, dynamics, and function. *Physiology (Bethesda)*, *25*(5), 293-303. https://doi.org/25/5/293 [pii]10.1152/physiol.00002.2010

Dorr, P., Westby, M., Dobbs, S., Griffin, P., Irvine, B., Macartney, M., . . . Perros, M. (2005). Maraviroc (UK-427,857), a potent, orally bioavailable, and selective small-molecule inhibitor of chemokine receptor CCR5 with broad-spectrum anti-human immunodeficiency virus type 1 activity. *Antimicrob Agents Chemother*, *49*(11), 4721-4732. http://www.ncbi.nlm.nih.gov/entrez/query.fcgi?cmd=Retrieve&db=PubMed&dopt=Citation&list_uids=16251317

Durrett, R. (2018). *Stochastic calculus: a practical introduction*. CRC press.

Escola, J. M., Kuenzi, G., Gaertner, H., Foti, M., & Hartley, O. (2010). CC chemokine receptor 5 (CCR5) desensitization: cycling receptors accumulate in the trans-Golgi network. *J Biol Chem*, *285*(53), 41772-41780. https://doi.org/M110.153460 [pii]10.1074/jbc.M110.153460

Fillion, D., Devost, D., Sleno, R., Inoue, A., & Hebert, T. E. (2019). Asymmetric Recruitment of beta-Arrestin1/2 by the Angiotensin II Type I and Prostaglandin F2alpha Receptor Dimer. *Front Endocrinol (Lausanne)*, *10*, 162. https://doi.org/10.3389/fendo.2019.00162

Flanagan, C. A. (2014). Receptor conformation and constitutive activity in CCR5 chemokine receptor function and HIV infection. *Adv Pharmacol*, *70*, 215-263. https://doi.org/10.1016/B978-0-12-417197-8.00008-0

Fox, J. M., Kasprowicz, R., Hartley, O., & Signoret, N. (2015). CCR5 susceptibility to ligand-mediated down-modulation differs between human T lymphocytes and myeloid cells. *J Leukoc Biol*, *98*(1), 59-71. https://doi.org/10.1189/jlb.2A0414-193RR

Garcia-Perez, J., Rueda, P., Staropoli, I., Kellenberger, E., Alcami, J., Arenzana-Seisdedos, F., & Lagane, B. (2011). New Insights into the Mechanisms whereby Low Molecular Weight CCR5 Ligands Inhibit HIV-1 Infection. *J Biol Chem*, *286*(7), 4978-4990. http://www.ncbi.nlm.nih.gov/entrez/query.fcgi?cmd=Retrieve&db=PubMed&dopt=Citation&list_uids=21118814

Gormal, R. S., Padmanabhan, P., Kasula, R., Bademosi, A. T., Coakley, S., Giacomotto, J., . . . Meunier, F. A. (2020). Modular transient nanoclustering of activated beta2-adrenergic receptors revealed by single-molecule tracking of conformation-specific nanobodies. *Proc Natl Acad Sci U S A*, *117*(48), 30476-30487. https://doi.org/10.1073/pnas.2007443117

Grove, J., Metcalf, D. J., Knight, A. E., Wavre-Shapton, S. T., Sun, T., Protonotarios, E. D., . . . Marsh, M. (2014). Flat clathrin lattices: stable features of the plasma membrane. *Mol Biol Cell*, *25*(22), 3581-3594. https://doi.org/10.1091/mbc.E14-06-1154

Irannejad, R., Tomshine, J. C., Tomshine, J. R., Chevalier, M., Mahoney, J. P., Steyaert, J., . . . von Zastrow, M. (2013). Conformational biosensors reveal GPCR signalling from endosomes. *Nature*, *495*(7442), 534-538. https://doi.org/10.1038/nature12000

Isbilir, A., Moller, J., Arimont, M., Bobkov, V., Perpina-Viciano, C., Hoffmann, C., . . . Lohse, M. J. (2020). Advanced fluorescence microscopy reveals disruption of dynamic CXCR4 dimerization by subpocket-specific inverse agonists. *Proc Natl Acad Sci U S A*, *117*(46), 29144-29154. https://doi.org/10.1073/pnas.2013319117

914 Jacquemard, C., Koensgen, F., Colin, P., Lagane, B., & Kellenberger, E. (2021). Modeling of
915 CCR5 Recognition by HIV-1 gp120: How the Viral Protein Exploits the Conformational
916 Plasticity of the Coreceptor. *Viruses*, *13*(7). https://doi.org/10.3390/v13071395
917 Jin, J., Colin, P., Staropoli, I., Lima-Fernandes, E., Ferret, C., Demir, A., . . . Brelot, A. (2014).
918 Targeting Spare CC Chemokine Receptor 5 (CCR5) as a Principle to Inhibit HIV-1 Entry.
919 *J Biol Chem*, *289*(27), 19042-19052. https://doi.org/M114.559831
920 [pii]10.1074/jbc.M114.559831

921 Jin, J., Momboisse, F., Boncompain, G., Koensgen, F., Zhou, Z., Cordeiro, N., . . . Brelot, A.
922 (2018). CCR5 adopts three homodimeric conformations that control cell surface delivery.
923 *Sci Signal*, *11*(529). https://doi.org/10.1126/scisignal.aal2869
924 Kasai, R. S., Ito, S. V., Awane, R. M., Fujiwara, T. K., & Kusumi, A. (2018). The Class-A GPCR
925 Dopamine D2 Receptor Forms Transient Dimers Stabilized by Agonists: Detection by
926 Single-Molecule Tracking. *Cell Biochem Biophys*, *76*(1-2), 29-37.
927 https://doi.org/10.1007/s12013-017-0829-y
928 Lagane, B., Ballet, S., Planchenault, T., Balabanian, K., Le Poul, E., Blanpain, C., . . . Bachelerie,
929 F. (2005). Mutation of the DRY motif reveals different structural requirements for the CC
930 chemokine receptor 5-mediated signaling and receptor endocytosis. *Mol Pharmacol*,
931 *67*(6), 1966-1976. https://doi.org/mol.104.009779 [pii]10.1124/mol.104.009779

932 Martinez-Munoz, L., Rodriguez-Frade, J. M., Barroso, R., Sorzano, C. O. S., Torreno-Pina, J. A.,
933 Santiago, C. A., . . . Mellado, M. (2018). Separating Actin-Dependent Chemokine
934 Receptor Nanoclustering from Dimerization Indicates a Role for Clustering in CXCR4
935 Signaling and Function. *Mol Cell*, *71*(5), 873. https://doi.org/10.1016/j.molcel.2018.08.012
936 Maurice, P., Daulat, A. M., Turecek, R., Ivankova-Susankova, K., Zamponi, F., Kamal, M., . . .
937 Jockers, R. (2010). Molecular organization and dynamics of the melatonin MT(1)
938 receptor/RGS20/G(i) protein complex reveal asymmetry of receptor dimers for RGS and
939 G(i) coupling. *EMBO J*, *29*(21), 3646-3659. https://doi.org/10.1038/emboj.2010.236
940 Moller, J., Isbilir, A., Sungkaworn, T., Osberg, B., Karathanasis, C., Sunkara, V., . . . Lohse, M. J.
941 (2020). Single-molecule analysis reveals agonist-specific dimer formation of micro-opioid
942 receptors. *Nat Chem Biol*, *16*(9), 946-954. https://doi.org/10.1038/s41589-020-0566-1
943 Olivo-Marin, J.-C. (2002). Extraction of spots in biological images using multiscale products.
944 *Pattern recognition*, *35*(9), 1989-1996.
945 Patwardhan, A., Cheng, N., & Trejo, J. (2021). Post-Translational Modifications of G Protein-
946 Coupled Receptors Control Cellular Signaling Dynamics in Space and Time. *Pharmacol*
947 *Rev*, *73*(1), 120-151. https://doi.org/10.1124/pharmrev.120.000082
948 Pierce, K. L., Premont, R. T., & Lefkowitz, R. J. (2002). Seven-transmembrane receptors. *Nat*
949 *Rev Mol Cell Biol*, *3*(9), 639-650. https://doi.org/10.1038/nrm908
950 Qian, H., Sheetz, M. P., & Elson, E. L. (1991). Single particle tracking. Analysis of diffusion and
951 flow in two-dimensional systems. *Biophys J*, *60*(4), 910-921.
952 https://doi.org/10.1016/S0006-3495(91)82125-7
953 Salavessa, L., Lagache, T., Malarde, V., Grassart, A., Olivo-Marin, J. C., Canette, A., . . .
954 Sauvonnet, N. (2021). Cytokine receptor cluster size impacts its endocytosis and
955 signaling. *Proc Natl Acad Sci U S A*, *118*(37). https://doi.org/10.1073/pnas.2024893118
956 Scurci, I., Akondi, K. B., Pinheiro, I., Paolini-Bertrand, M., Borgeat, A., Cerini, F., & Hartley, O.
957 (2021). CCR5 tyrosine sulfation heterogeneity generates cell surface receptor
958 subpopulations with different ligand binding properties. *Biochim Biophys Acta Gen Subj*,
959 *1865*(1), 129753. https://doi.org/10.1016/j.bbagen.2020.129753
960 Seyedabadi, M., Ghahremani, M. H., & Albert, P. R. (2019). Biased signaling of G protein coupled
961 receptors (GPCRs): Molecular determinants of GPCR/transducer selectivity and
962 therapeutic potential. *Pharmacol Ther*, *200*, 148-178.
963 https://doi.org/10.1016/j.pharmthera.2019.05.006
964 Shaik, M. M., Peng, H., Lu, J., Rits-Volloch, S., Xu, C., Liao, M., & Chen, B. (2019). Structural
965 basis of coreceptor recognition by HIV-1 envelope spike. *Nature*, *565*(7739), 318-323.
966 https://doi.org/10.1038/s41586-018-0804-9

967 Sleno, R., & Hebert, T. E. (2018). The Dynamics of GPCR Oligomerization and Their Functional
968 Consequences. *Int Rev Cell Mol Biol*, *338*, 141-171.
969 https://doi.org/10.1016/bs.ircmb.2018.02.005
970 Sohy, D., Yano, H., de Nadai, P., Urizar, E., Guillabert, A., Javitch, J. A., . . . Springael, J. Y.
971 (2009). Hetero-oligomerization of CCR2, CCR5, and CXCR4 and the protean effects of
972 "selective" antagonists. *J Biol Chem*, *284*(45), 31270-31279.
973 http://www.ncbi.nlm.nih.gov/entrez/query.fcgi?cmd=Retrieve&db=PubMed&dopt=Citation
974 &list_uids=19758998
975 Sungkaworn, T., Jobin, M. L., Burnecki, K., Weron, A., Lohse, M. J., & Calebiro, D. (2017).
976 Single-molecule imaging reveals receptor-G protein interactions at cell surface hot spots.
977 *Nature*, *550*(7677), 543-547. https://doi.org/10.1038/nature24264
978 Tabor, A., Weisenburger, S., Banerjee, A., Purkayastha, N., Kaindl, J. M., Hubner, H., . . .
979 Gmeiner, P. (2016). Visualization and ligand-induced modulation of dopamine receptor
980 dimerization at the single molecule level. *Sci Rep*, *6*, 33233.
981 https://doi.org/10.1038/srep33233
982 Tilton, J. C., Wilen, C. B., Didigu, C. A., Sinha, R., Harrison, J. E., Agrawal-Gamse, C., . . . Doms,
983 R. W. (2010). A maraviroc-resistant HIV-1 with narrow cross-resistance to other CCR5
984 antagonists depends on both N-terminal and extracellular loop domains of drug-bound
985 CCR5. *J Virol*, *84*(20), 10863-10876. https://doi.org/10.1128/JVI.01109-10
986 Vangelista, L., & Vento, S. (2017). The Expanding Therapeutic Perspective of CCR5 Blockade.
987 *Front Immunol*, *8*, 1981. https://doi.org/10.3389/fimmu.2017.01981
988 Veya, L., Piguet, J., & Vogel, H. (2015). Single Molecule Imaging Deciphers the Relation between
989 Mobility and Signaling of a Prototypical G Protein-coupled Receptor in Living Cells. *J Biol*
990 *Chem*, *290*(46), 27723-27735. https://doi.org/10.1074/jbc.M115.666677
991 Whorton, M. R., Bokoch, M. P., Rasmussen, S. G., Huang, B., Zare, R. N., Kobilka, B., &
992 Sunahara, R. K. (2007). A monomeric G protein-coupled receptor isolated in a high-
993 density lipoprotein particle efficiently activates its G protein [Research Support, N.I.H.,
994 Extramural Research Support, Non-U.S. Gov't Research Support, U.S. Gov't, Non-
995 P.H.S.]. *Proc Natl Acad Sci U S A*, *104*(18), 7682-7687.
996 https://doi.org/10.1073/pnas.0611448104

997 Yanagawa, M., Hiroshima, M., Togashi, Y., Abe, M., Yamashita, T., Shichida, Y., . . . Sako, Y.
998 (2018). Single-molecule diffusion-based estimation of ligand effects on G protein-coupled
999 receptors. *Sci Signal*, *11*(548). https://doi.org/10.1126/scisignal.aao1917

1000

Figure supplement

Single-molecule imaging reveals distinct effects of ligands on CCR5 dynamics depending on its dimerization status.

Fanny Momboisse[1], Giacomo Nardi[2], Philippe Colin[3], Melany Hery[1], Nelia Cordeiro[1], Olivier Schwartz[1], Nathalie Sauvonnet[5], Fernando Arenzana-Seisdedos[4], Thibault Lagache[2*], Bernard Lagane[3], Jean-Christophe Olivo-Marin[2], Anne Brelot[1*]

Corresponding author: Anne Brelot and Thibault Lagache
Anne Brelot: anne.brelot@pasteur.fr

Thibault Lagache: thibault.lagache@pasteur.fr

This PDF file includes:

Other materials for this manuscript include the following:

Video 1
Video 2
Video 3
Video 4
Video 5
Video 6

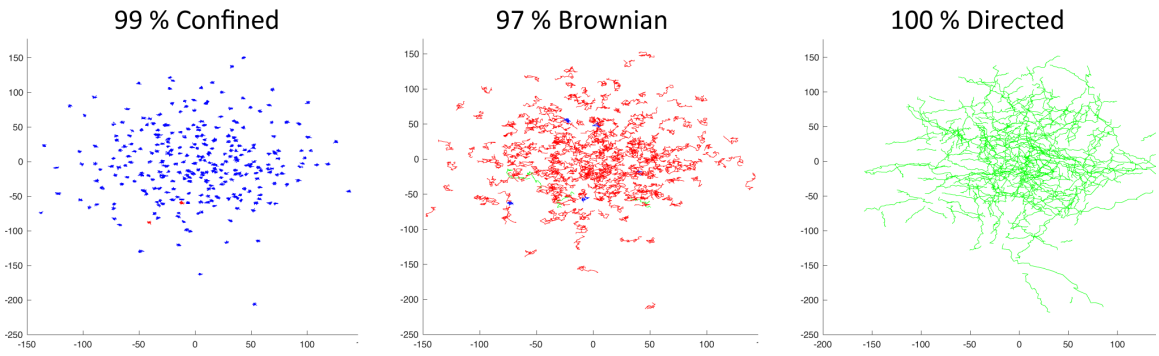

Figure 1-figure supplement 1. Validation of the statistical method using simulated trajectories. The three motions, confined, Brownian, and directed, were simulated by Monte Carlo experiments. For each type of motion, we simulated 300 tracks with length 11, with a Matlab program by using equations given in Materials and Methods. Trajectories were classified with the statistical method. The parameters used for the statistical classification were the following: N=10, α=0.05, q(α)=0.725, and q(1- α) = 2.626. The percentage of detection of the different trajectories were indicated.

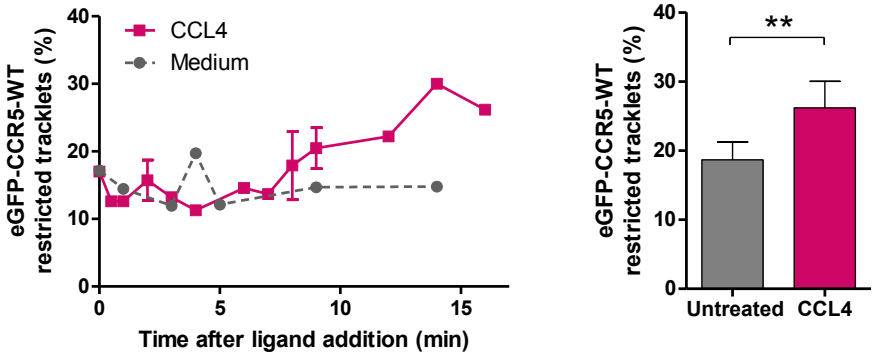

Figure 3-figure supplement 1: Effect of CCL4 on CCR5 mobility. eGFP-CCR5-WT expressing cells were treated or not with a saturating concentration of CCL4 (200 nM) and single particle tracking analysis was performed. Percentage of restricted tracklets after treatment over time (left) and after 12 to 16 min of treatment (right) (mean ± SD, n= 9 951 and 4 320 tracks for untreated and CCL4 conditions, from 6 and 3 cells respectively). Unpaired t test: p value 0.0088**.

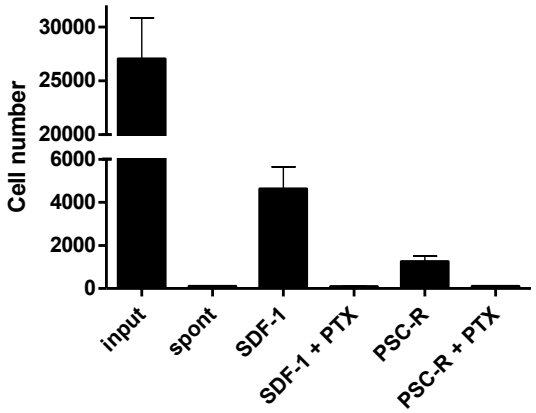

Figure 4-figure supplement 1. Effect of PTX treatment on chemokine-mediated chemotaxis. A3.01-R5 cells treated with 100 ng/ml PTX for 3 h were added to the upper chambers of HTS-transwell. Chemokines were to the lower chambers and chemotaxis were proceeded for 4 h. The number of cells migrating across the membrane was assessed by flow cytometry. PTX-treatment impaired SDF-1 (10 nM) and PSC-RANTES (33.7 nM)-mediated chemotaxis of A3.01-R5 cells. One representative experiment of 2 independent experiments (mean ± SD of triplicates). *Spont:* Spontaneous migration (without chemokines in the lower chamber).

Videos legends

Video 1. TIRF movie of a cell stably expressing eGFP-CCR5-WT acquired at 30 Hz. The region of interest was defined by the green line**.**

Video 2. TIRF movie of the same cell as in video 1 analyzed using the Icy software. Red circles correspond to the detection of bright spots using the *Spot detection* pluggin*.*

Video 3. TIRF movie of the same cell as in video 1 and 2 analyzed using the Icy software and the *Spot tracking* pluggin. Colored lines correspond to the tracked spots.

Video 4. TIRF movie acquired at 30 Hz of a cell stably expressing eGFP-CCR5-WT and treated by CCL4 (100 nM) for 14 min.

Video 5. TIRF movie acquired at 30 Hz of cells stably expressing eGFP-CCR5-WT and treated by PSC-RANTES (20 nM) for 3 min.

Video 6. TIRF movie acquired at 30 Hz of a cell stably expressing eGFP-CCR5-L196K and treated by PSC-RANTES (20 nM) for 2 min.